

# Quantum computing in neural networks

P. GRALEWICZ

Department of Theoretical Physics, University of Łódź, Pomorska 149/153, 90-236, Łódź, Poland

## Abstract

According to the statistical interpretation of quantum theory, quantum computers form a distinguished class of probabilistic machines (PMs) by encoding  $n$  qubits in  $2n$  pbits. This raises the possibility of a large-scale quantum computing using PMs, especially with neural networks which have the innate capability for probabilistic information processing. Restricting ourselves to a particular model, we construct and numerically examine the performance of neural circuits implementing universal quantum gates. A discussion on the physiological plausibility of proposed coding scheme is also provided.

## 1 Introduction

Neural networks are naturally evolved systems for information processing. Despite decades of experimental and theoretical research, there is no agreement upon the information encoding employed by these circuits and the problem of what exactly is being communicated *via* seemingly chaotic spike trains is still largely open [1]. Advancement in understanding of this neural language is obstructed by variety of cell types, working conditions and molecular factors to be taken into account [2]. Generally accepted schemes, the *rate code* and the *phase code*, may turn out to be only the first two in a sequence of progressively more intricate codes, where higher order correlations within cellular complexes are utilized.

Quantum information science, on the other hand, had matured over the last two decades making significant contributions to both information theory and quantum mechanics (QM). The latter, having historical roots in particle physics, is still often identified with the micro-world. Yet, there is nothing in the mathematical foundations of QM which could justify that point of view. In fact, apart from that microscopic realizations, quantum theory has found many avatars, from mechanical [3], linguistic [4], purely geometric [5], to statistical [6, 7, 8, 9]. In this article, that last, widely accepted interpretation, is being used to study the feasibility of a hypothesis that spike trains may actually encode for quantum states.

The hypothesis appears particularly attractive in that the Nature is notorious in repeating itself at various scales, and if quantum computing (QC) proves to be practical, it would be rather surprising if one could not find it implemented at a higher level. From this point of view neural networks are the obvious candidates to look for such implementations. By examining two neural circuits, designed to perform quantum operations (1-qubit rotations, and 2-qubit CNOT gate), we demonstrate the feasibility of our hypothesis within the limits of a simple model. Although quantum registers are realized efficiently, with just two neurons per qubit, the major costs are in the processing of information carried by the spike trains. The simulations provided are intended to emphasize the amount of these resources as well as the function-

ality required for implementation.

We commence with a short review of the formalism which permits to identify pairs of spiking neurons with qubits. In Section 3 a reduced model of neural network is described, which further, in Sec. 4 is used as a basis for construction of quantum gates. The results of simulations, in terms of achieved fidelity and coherence, are promising enough to look toward more realistic implementations. We touch briefly on these issues in the last section.

## 2 Manipulation of quantum states embedded in probabilistic space

The formalism of positive operator-valued measures (POVMs), allows one to express the states of a quantum system defined in a finite-dimensional Hilbert space  $H$ , in terms of probability distributions. If the dimension is  $d = \dim H$ , then a generic density matrix  $\rho$  representing the state has  $d^2 - 1$  degrees of freedom (DOFs). A distribution obtained through particular POVM has length  $d^2$ , and – due to normalization constraint – the same number of DOFs as the density matrix [8]. For  $n$ -qubit states, this distribution can be associated with joint probability of  $2n$  binary random variables<sup>1</sup>.

Let  $\rho$  be a generic density matrix of a 1-qubit state, which using summation convention, we write as

$$\rho = \rho^z = \begin{matrix} \frac{1}{2} + \frac{\rho^3}{2} & \frac{\rho^1}{2} + \frac{\rho^2}{2} \\ \frac{\rho^1}{2} & \frac{1}{2} - \frac{\rho^3}{2} \end{matrix};$$

where  $\rho_0 = 1$ ,  $\rho_{1,2,3}$  are the Pauli matrices,  $\rho^0 = \frac{1}{2}$ , and  $\rho^1, \rho^2, \rho^3 \in [\frac{1}{2}, \frac{1}{2}]$  are the three real coordinates of a Bloch vector. Let  $\hat{A}^z$  be a normalized 4-element positive operator-valued measure

$$\sum_z \hat{A}^z = 1; \quad z = 0, \dots, 3; \quad (1)$$

Typically, one associates such a POVM with the Pauli basis, that is

$$\hat{A}^z = A^z \wedge = \frac{1}{2} \mathbb{1} + A^z_i \wedge^i; \quad i = 1, \dots, 3;$$

<sup>1</sup>This is in close analogy to complex numbers which extend the reals, and at the same time are embeddable in a real vector space of doubled dimension equipped with complex structure.



independent measure by which one can estimate the angular disparity between expected and obtained states. The *fidelity*, or normalized overlap between  $\hat{p} \in \mathbb{R}^{2^n}$  and  $\hat{q} \in \mathbb{R}^{2^n}$  is defined here as

$$F = \frac{g(\hat{p}; \hat{q})}{g(\hat{p}; \hat{p}) g(\hat{q}; \hat{q})};$$

We choose fidelity as a commonly adopted measure, for the purpose of comparison, despite a direct estimate of the unitary error between the desired pure state  $\hat{p} \in \mathbb{R}^{2^n}$  and obtained distribution  $\hat{q} \in \mathbb{R}^{2^n}$  is readily computable by

$$= \arccos \frac{g(\hat{p}; \hat{q})}{r(\hat{q})} \frac{2^n}{2^n - 1};$$

The two quantities  $r(\hat{q})$  and  $F$ , are nevertheless dependent.

### 3 A toy-model neural-network

The information in neural networks is carried by spike trains, which after appropriate discretization can be transformed to binary strings. The model network described in this section is a much simplified version of what usually is considered realistic – the purpose of such reduction is to retain only the essential features. Consistently with discretization of transmitted signals, we run the model in a step-wise manner rather than seeking continuous-time evolution. The delays effected along the inter-neuron paths are also taken to be integers<sup>3</sup>.

Let  $G = (V; E)$ , be a multiply-connected digraph, where  $V = \{v_i\}_{i=1}^N$  is the vertex basis of neurons, (we shall also write  $V_N$  to explicit the number  $N$  of vertices involved) and  $E = \{e_{ij}\}_{i,j=1}^N$  is the basis of edges, that is the possible synaptic connections. The actual couplings between  $i^{th}$  and  $j^{th}$  neuron are set by the weights  $w_{ij}$ , where  $s \in \mathbb{N}$  enumerates the delays introduced along multiple edges. For each vertex we define two variables: the binary *output state*  $X \in \{0, 1\}^V$ , and the *latent potential*  $u \in \mathbb{R}^V$ .

We adopt the discrete *integrate-and-fire* scheme for the dynamics of this network. In each time step the potential is first updated by accumulating the incoming signals

$$u^{it+1} \leftarrow u_i^{it} + \sum_j w_{ij} X_{jt} s$$

where the summation runs over connected vertices ( $j$ ) and edge delays ( $s > 1$ ). Subsequent spike generation ( $X_{jt} = 1$ ) occurs with probability  $P(u_i^{it})$ , where  $P : \mathbb{R} \rightarrow [0, 1]$  is a ‘noisy’ activation function with firing threshold fixed at  $u_{thr} = \frac{1}{2}$ . Its actual form used in simulations is given by

$$P(u_i) = \frac{1}{2} \left( 1 + \text{erf} \frac{u_i - u_{thr}}{\sqrt{2}} \right);$$

<sup>3</sup>This latter feature can, to some extent be justified by the physiology of neural connections: The difference in propagation speed of action potentials between myelin-sheathed and unsheathed parts of an axon are at least one order of magnitude. The introduced delays are therefore dominated by the number of unsheathed segments which is roughly an integer.

where  $\sigma > 0$  is a global control parameter characterizing the noise standard deviation (SD). In particular, in the limit  $\sigma \rightarrow 0$  the spikes are produced deterministically, as  $P$  becomes a step-function. The excited state  $u_i^{it}$  is eventually reduced by release of a spike, and further quenched with a bound, nonlinear map  $S$

$$u_i^{it+1} = S(u_i^{it}) = S(u_i^{it} - X_{it});$$

We assume  $S$  to have an attractive fixed point at the origin (the resting potential),  $S_u : \lim_{t \rightarrow \infty} S^t(u) = 0$ , to be linear in its neighborhood  $S'(0) = 1$ , and having finite, but non-zero asymptotes  $S(-1) = 1$ . The motivation for introduction of this mapping is twofold: First, the physiological mechanisms of signal transmission imply existence of *saturations* in both positive and negative direction. The cell can be depolarized or hyperpolarized through synaptic channels only to certain extent, and adding more excitatory or inhibitory connections will not have a significant effect. Second, the reason to have  $u = 0$  for an attractive fixed point, is to imitate the ‘leaky’ integration scenario, by which in the absence of input the potential returns back to its resting point. In the simulations this function was taken to be a simple, skew-symmetric mapping

$$S(u) = \tanh \frac{u}{\sigma}; \quad u > 0;$$

Here, the asymptotes are  $S(-1) = 1$ , therefore we call  $\sigma$  the ‘saturation parameter’. If we assume the neuron is left without input and some residual  $u$ , so that no spikes are generated, then the potential  $u$  will decay sub-exponentially in time, as

$$u^{it+1} = S^t(u) \approx \frac{u}{1 + \frac{2}{3} \sigma^2 t^2};$$

where  $S^t$  means  $t$ -fold composition. In the limit  $\sigma \rightarrow 0$ , the latent potential is reset to zero after each cycle, and this situation can be associated with time steps longer than the refractory time, within which each cell relaxes to its resting point. The choice of a specific value of  $\sigma$  is therefore indirectly related to the time step in this model, and consequently to the discretization window of action potentials. If this window is too short, the discretization becomes ambiguous and the model breaks down – this is one of the reasons not to consider high saturation values. Another comes from the mechanisms of spike generation, by which multiple spikes within the refractory period are suppressed.

The qualitative behavior of the above model is best understood by analyzing single neuron at the limits of the two control parameters  $\sigma$  and  $\tau$ . Assume the cell is fed with a stimulus at a constant frequency  $\tau \in [0, 1]$  and consider at first the noiseless regime  $\sigma = 0$ . If  $\tau = 0$ ,

then the only memory of past input values is stored in delayed connections. The cell fires only if the value of the convolution  $W_{js} x^{jt} s$  exceeds the threshold  $u_{thr}$ . Such neurons acts like a high-pass filter and its firing rate is  $P_{out} = P(\text{in}_{s;j} W_{js})$ . By increasing the noise SD  $\sigma$ , the shape of this filtering function changes along with the spiking probability  $P$ , nevertheless it never becomes close to an ideal multiplier – the response is always non-linear.

If  $\sigma \neq 1$  the cell accumulates and ‘remembers’ the residual value of convolution left over after subtraction of generated spikes. This makes it into a perfect multiplier with spike rate  $P_{out} = \text{in}_{s;j} W_{js}$ . Raising  $\sigma$  above zero does not change this average response, but the determinism initially apparent in the spike patterns is gradually being washed away.

In between of these two regimes, lies a surprisingly complex area of fractal-spaced frequency thresholds and output patterns, particularly conspicuous at  $\sigma = 0$  and  $\sigma = 1$ . Presence of these features, found in many non-linear deterministic systems do not critically depend on the specific shape of the function  $S$ .

## 4 Implementation of universal quantum gates

According to the discussion provided in section 2, one needs  $2n$  random binary variables to implement an  $n$ -qubit register. In our model of the neural network, these variables are identified with discretized spikes registered at  $2n$  network sites. The question we set up to address in this section is, whether there are circuits which can implement state-independent rotations of the joint probability distributions, that is – quantum gates.

The set of gates universal for quantum computation [12] includes the whole algebra of 1-qubit rotations, and an arbitrary 2-qubit entangling gate, typically chosen to be the CNOT (controlled-NOT). Although probabilistic encoding of qubits is efficient (*i.e.* linear in  $n$ ), manipulation of their  $2^{2n}$  degrees of freedom (DOFs), by definition requires exponential amount of resources. From this perspective the construction of circuits described below should appear at least conceptually straightforward: The space of binary functions over the vertices  $V_{2n}$  is  $V^{2n} = \mathbb{Z}_{2n}$ . We first embed an element  $X^t = fX^{it} g 2 V^{2n}$  into  $\mathbb{Z}_{2n}$ , then apply the gate  $G = A L A^{-1}$ , and finally project the result back onto  $V^{2n}$ . The entire quantum gate transforming one set of spike trains  $X^t$  to another  $Y^t \in V^{2n}$ , is then a composition

$$G = A L A^{-1} : X^t \mapsto Y^t;$$

where  $A^{-1} : V^{2n} \rightarrow \mathbb{Z}_{2n}$ , and  $L^{-1} = \text{id}_{V^{2n}}$ . The main problem in this approach is to construct a reliable projection  $L$ , since any information loss during that operation will affect the quality of entire gate.

<sup>4</sup>With  $A$  given by (6), the 1-qubit NOT gate becomes a permutation  $(00;10)(01;11)$ , and can be implemented with high efficiency. An alternative choice associated with the real Fourier transform, brings the Hadamard’s gate  $H$  to a permutation, therefore if an algorithm relies on frequent applications of this operation, that could be a preferred choice.

Concrete realization, requires also to decide upon particular POVM being used. It is possible to choose this transformation in such a way, that some of the gates will be significantly simplified, for instance acquiring convenient form of permutations. Our choice is dictated by the optimization of the CNOT gate, discussed latter in this section. This POVM is given by<sup>4</sup>

$$A^z = \begin{bmatrix} 0 & 1 & \frac{1}{3} & \frac{1}{3} & \frac{1}{3} & 1 \\ \frac{1}{3} & 1 & \frac{1}{3} & \frac{1}{3} & \frac{1}{3} & C \\ \frac{1}{3} & \frac{1}{3} & 1 & \frac{1}{3} & \frac{1}{3} & A \\ \frac{1}{3} & \frac{1}{3} & \frac{1}{3} & 1 & \frac{1}{3} & B \\ \frac{1}{3} & \frac{1}{3} & \frac{1}{3} & \frac{1}{3} & 1 & B \\ 1 & \frac{1}{3} & \frac{1}{3} & \frac{1}{3} & \frac{1}{3} & \end{bmatrix} : \quad (6)$$

### 4.1 Single-qubit gates

The neural circuit implementing arbitrary 1-qubit gate is presented in Fig. 1. The projection  $W$  which transforms the ‘sparse’ code  $fX^{00}; X^{01}; X^{10}; X^{11} g 2 V^2$  onto a ‘dense’ one  $fX^A; X^B g 2 V^2$ , is a linear mapping implemented with weights

$$W = \begin{bmatrix} 0 & 0 & 1 & 1 \\ 0 & 1 & 0 & 1 \end{bmatrix} :$$

But its inverse,  $W^{-1}$  is nonlinear and we realize this function, in a two-step linear-feedback operation. The first step requires, apart from the input signals, an additional supply of constant ‘current’ of units from the vertex  $v_1$ . The effect of such a coupling to unity on a cell is to alter its firing threshold. The weights of this part, effecting a linear injection from  $fX^A; X^B; 1 g$  to  $fX^{00}; X^{01}; X^{10}; X^{11} g$  are

$$W^{-1} = \begin{bmatrix} 0 & 1 & 1 & 1 \\ \frac{1}{3} & 1 & 1 & 0 \\ \frac{1}{3} & 1 & 1 & 0 \\ 1 & 1 & 1 & 1 \end{bmatrix} :$$

While the composition  $W \circ W^{-1} = \text{id}_{V^2}$  as required, the reciprocal is not an identity and needs a rectifying feedback sent from the ‘winning’ neuron to its neighbors, in order to bring their latent potentials back to zero. Because of the one-step delay, this signal has to be adjusted to match the attenuation already done by the function  $S$ . Hence the weight matrix of this rectification step is determined by

$$W_{\text{rec}}^i j = S W^{-1} W^i j = S (1) \mathbb{1}_2 W^{-1} W^i j : \quad (7)$$

Note, that for vanishing saturation parameter, this correction also disappears due to  $S = 0$ .

In the absence of noise ( $\sigma = 0$ ), the conversion  $W^{-1}$  between dense and sparse coding is completely error-free. As  $\sigma$  increases, the imperfections start to appear

in the form of either multiple, or void spiking in the first hidden layer. Although we found the circuit to behave stably in these conditions, an improvement, in terms of both fidelity and coherence, can be achieved by adding a second, normalizing feedback (not shown explicitly in Fig. 1).

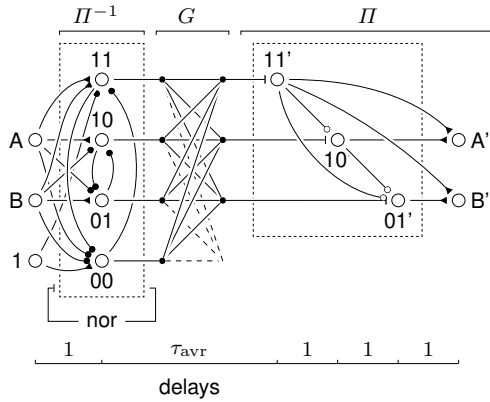


**Figure 1** Schematic for the 1-qubit gate. The hidden nodes are drawn in inverted lexicographical order to avoid excessive entanglement of the graph. Explicit connections of the normalization (nor) feedback were omitted, to improve legibility. Inhibitory connections are marked with  $(-)$ , excitatory – with  $(+)$ , and those capped with  $(\rightarrow)$  depend on the applied gate  $G$ . The double connections  $(\rightarrow)$  consist of inhibition followed by delayed and attenuated excitation. The transient time is  $\tau_{\text{gate}} = 4 + \tau_{\text{avr}}$ . Including the normalization feedback, and doubled gate connections ( $\tau_{\text{avr}} = 2$ ), the circuit comprises 10 nodes, and 62 edges.

Normalizing feedbacks are commonly proposed for explanation of the observed behavior in cortical neurons [16, 17]. The main difference between these and our proposal is that while the former are multiplicative, this one acts additively. Its role is to adjust the latent potentials for the difference

$$\frac{X}{1} = \frac{X^i}{i}; \quad i = 00; 01; 10; 11;$$

Because we do not know which of the four neurons spiked mistakenly, the normalizing signal is sent evenly to all of them. Its strength is determined by the average excess of a signal encountered on a double spike event:

$$\frac{X}{4} = \frac{W_{\text{rec}}^i}{j} = \frac{1}{4} S(-1);$$

The same in amount but with opposite sign is the deficit, which happens upon lack of a single spike. Therefore, the weight matrix of this normalization reads

$$W_{\text{nor}} = S(-1) \begin{bmatrix} 0 & \frac{1}{4} & \frac{1}{4} & \frac{1}{4} & \frac{1}{4} & 1 \\ B & \frac{1}{4} & \frac{1}{4} & \frac{1}{4} & \frac{1}{4} & 1 \\ B & \frac{1}{4} & \frac{1}{4} & \frac{1}{4} & \frac{1}{4} & 1 \\ B & \frac{1}{4} & \frac{1}{4} & \frac{1}{4} & \frac{1}{4} & 1 \\ B & \frac{1}{4} & \frac{1}{4} & \frac{1}{4} & \frac{1}{4} & 1 \end{bmatrix};$$

where the last column refers to the unit vertex  $v_1$ .

Making the embedding  $\mathbb{C}^4$  robust is crucial for achieving correct projection  $\mathbb{C}^4$ . Multiple, or void events linearly projected via  $W$  typically lead to a significant loss of coherence (although with less impact on fidelity).

In order to counter these non-exclusive events, the spiking neuron sends a composite inhibitory signal down the hierarchy. This is implemented with double connections: the first transmits inhibitory signal at certain level  $\tau_{\text{avr}}$ , and is followed by a delayed, excitatory one aimed at bringing the latent potential of receiving neuron back to its prior value. The full accomplishment of this goal is impossible with nonlinear function  $S$  – the value can only be fully restored in the linear limit  $\tau_{\text{avr}} = 1$ . Given the inhibitory coupling  $\tau_{\text{avr}}$ , our best estimate of the following excitation strength is  $\tau_{\text{avr}} = h_{\text{ui}} S(h_{\text{ui}} \tau_{\text{avr}})$ , where  $h_{\text{ui}}$  is the average latent potential. Because  $h_{\text{ui}} \approx 0$ , we set  $\tau_{\text{avr}} = S(0)$ . The optimal value of  $\tau_{\text{avr}}$  was found numerically, by minimizing the variation of fidelity over a range of gates acting on test states (see Results).

Application of a gate  $G$  does not require any additional node of the network, but only manipulation of the weights between the embedding and projecting parts. In simplest case these are directly set to

$$W_G = A L A^{-1} = G;$$

We have found however, that the mechanism of *synaptic averaging* may, within some limits, provide improvement of the performance. In real networks single synapse contribute only a tiny fraction of the total input signal [2]. Multiple connections of similar lengths lead to signal accumulation, while different delays – temporal averaging. In our toy-model, the first case is replaced by single, but strong connections, while for implementation of the latter we directly use several edges having different lengths with proportionately attenuated couplings. In the case of a single-qubit gate, of the several configurations tested, the best results were obtained with just two-step average  $\tau_{\text{avr}} = 2$ , hence, the connections were fixed at  $W_{G,1} = W_{G,2} = \frac{1}{2} G$ .

**Results.** In order to reduce statistical uncertainties, all gates were tested on a fixed set of 14 pure states approximately evenly distributed on the Bloch sphere:

$$\begin{aligned} & \frac{1}{4} \sum_{i=0}^3 \sum_{j=0}^3 \sum_{k=0}^3 \sum_{l=0}^3 \sum_{m=0}^3 \sum_{n=0}^3 \sum_{o=0}^3 \sum_{p=0}^3 \sum_{q=0}^3 \sum_{r=0}^3 \sum_{s=0}^3 \sum_{t=0}^3 \sum_{u=0}^3 \sum_{v=0}^3 \sum_{w=0}^3 \sum_{x=0}^3 \sum_{y=0}^3 \sum_{z=0}^3 \sum_{a=0}^3 \sum_{b=0}^3 \sum_{c=0}^3 \sum_{d=0}^3 \sum_{e=0}^3 \sum_{f=0}^3 \sum_{g=0}^3 \sum_{h=0}^3 \sum_{i=0}^3 \sum_{j=0}^3 \sum_{k=0}^3 \sum_{l=0}^3 \sum_{m=0}^3 \sum_{n=0}^3 \sum_{o=0}^3 \sum_{p=0}^3 \sum_{q=0}^3 \sum_{r=0}^3 \sum_{s=0}^3 \sum_{t=0}^3 \sum_{u=0}^3 \sum_{v=0}^3 \sum_{w=0}^3 \sum_{x=0}^3 \sum_{y=0}^3 \sum_{z=0}^3 \sum_{a=0}^3 \sum_{b=0}^3 \sum_{c=0}^3 \sum_{d=0}^3 \sum_{e=0}^3 \sum_{f=0}^3 \sum_{g=0}^3 \sum_{h=0}^3 \sum_{i=0}^3 \sum_{j=0}^3 \sum_{k=0}^3 \sum_{l=0}^3 \sum_{m=0}^3 \sum_{n=0}^3 \sum_{o=0}^3 \sum_{p=0}^3 \sum_{q=0}^3 \sum_{r=0}^3 \sum_{s=0}^3 \sum_{t=0}^3 \sum_{u=0}^3 \sum_{v=0}^3 \sum_{w=0}^3 \sum_{x=0}^3 \sum_{y=0}^3 \sum_{z=0}^3 \sum_{a=0}^3 \sum_{b=0}^3 \sum_{c=0}^3 \sum_{d=0}^3 \sum_{e=0}^3 \sum_{f=0}^3 \sum_{g=0}^3 \sum_{h=0}^3 \sum_{i=0}^3 \sum_{j=0}^3 \sum_{k=0}^3 \sum_{l=0}^3 \sum_{m=0}^3 \sum_{n=0}^3 \sum_{o=0}^3 \sum_{p=0}^3 \sum_{q=0}^3 \sum_{r=0}^3 \sum_{s=0}^3 \sum_{t=0}^3 \sum_{u=0}^3 \sum_{v=0}^3 \sum_{w=0}^3 \sum_{x=0}^3 \sum_{y=0}^3 \sum_{z=0}^3 \sum_{a=0}^3 \sum_{b=0}^3 \sum_{c=0}^3 \sum_{d=0}^3 \sum_{e=0}^3 \sum_{f=0}^3 \sum_{g=0}^3 \sum_{h=0}^3 \sum_{i=0}^3 \sum_{j=0}^3 \sum_{k=0}^3 \sum_{l=0}^3 \sum_{m=0}^3 \sum_{n=0}^3 \sum_{o=0}^3 \sum_{p=0}^3 \sum_{q=0}^3 \sum_{r=0}^3 \sum_{s=0}^3 \sum_{t=0}^3 \sum_{u=0}^3 \sum_{v=0}^3 \sum_{w=0}^3 \sum_{x=0}^3 \sum_{y=0}^3 \sum_{z=0}^3 \sum_{a=0}^3 \sum_{b=0}^3 \sum_{c=0}^3 \sum_{d=0}^3 \sum_{e=0}^3 \sum_{f=0}^3 \sum_{g=0}^3 \sum_{h=0}^3 \sum_{i=0}^3 \sum_{j=0}^3 \sum_{k=0}^3 \sum_{l=0}^3 \sum_{m=0}^3 \sum_{n=0}^3 \sum_{o=0}^3 \sum_{p=0}^3 \sum_{q=0}^3 \sum_{r=0}^3 \sum_{s=0}^3 \sum_{t=0}^3 \sum_{u=0}^3 \sum_{v=0}^3 \sum_{w=0}^3 \sum_{x=0}^3 \sum_{y=0}^3 \sum_{z=0}^3 \sum_{a=0}^3 \sum_{b=0}^3 \sum_{c=0}^3 \sum_{d=0}^3 \sum_{e=0}^3 \sum_{f=0}^3 \sum_{g=0}^3 \sum_{h=0}^3 \sum_{i=0}^3 \sum_{j=0}^3 \sum_{k=0}^3 \sum_{l=0}^3 \sum_{m=0}^3 \sum_{n=0}^3 \sum_{o=0}^3 \sum_{p=0}^3 \sum_{q=0}^3 \sum_{r=0}^3 \sum_{s=0}^3 \sum_{t=0}^3 \sum_{u=0}^3 \sum_{v=0}^3 \sum_{w=0}^3 \sum_{x=0}^3 \sum_{y=0}^3 \sum_{z=0}^3 \sum_{a=0}^3 \sum_{b=0}^3 \sum_{c=0}^3 \sum_{d=0}^3 \sum_{e=0}^3 \sum_{f=0}^3 \sum_{g=0}^3 \sum_{h=0}^3 \sum_{i=0}^3 \sum_{j=0}^3 \sum_{k=0}^3 \sum_{l=0}^3 \sum_{m=0}^3 \sum_{n=0}^3 \sum_{o=0}^3 \sum_{p=0}^3 \sum_{q=0}^3 \sum_{r=0}^3 \sum_{s=0}^3 \sum_{t=0}^3 \sum_{u=0}^3 \sum_{v=0}^3 \sum_{w=0}^3 \sum_{x=0}^3 \sum_{y=0}^3 \sum_{z=0}^3 \sum_{a=0}^3 \sum_{b=0}^3 \sum_{c=0}^3 \sum_{d=0}^3 \sum_{e=0}^3 \sum_{f=0}^3 \sum_{g=0}^3 \sum_{h=0}^3 \sum_{i=0}^3 \sum_{j=0}^3 \sum_{k=0}^3 \sum_{l=0}^3 \sum_{m=0}^3 \sum_{n=0}^3 \sum_{o=0}^3 \sum_{p=0}^3 \sum_{q=0}^3 \sum_{r=0}^3 \sum_{s=0}^3 \sum_{t=0}^3 \sum_{u=0}^3 \sum_{v=0}^3 \sum_{w=0}^3 \sum_{x=0}^3 \sum_{y=0}^3 \sum_{z=0}^3 \sum_{a=0}^3 \sum_{b=0}^3 \sum_{c=0}^3 \sum_{d=0}^3 \sum_{e=0}^3 \sum_{f=0}^3 \sum_{g=0}^3 \sum_{h=0}^3 \sum_{i=0}^3 \sum_{j=0}^3 \sum_{k=0}^3 \sum_{l=0}^3 \sum_{m=0}^3 \sum_{n=0}^3 \sum_{o=0}^3 \sum_{p=0}^3 \sum_{q=0}^3 \sum_{r=0}^3 \sum_{s=0}^3 \sum_{t=0}^3 \sum_{u=0}^3 \sum_{v=0}^3 \sum_{w=0}^3 \sum_{x=0}^3 \sum_{y=0}^3 \sum_{z=0}^3 \sum_{a=0}^3 \sum_{b=0}^3 \sum_{c=0}^3 \sum_{d=0}^3 \sum_{e=0}^3 \sum_{f=0}^3 \sum_{g=0}^3 \sum_{h=0}^3 \sum_{i=0}^3 \sum_{j=0}^3 \sum_{k=0}^3 \sum_{l=0}^3 \sum_{m=0}^3 \sum_{n=0}^3 \sum_{o=0}^3 \sum_{p=0}^3 \sum_{q=0}^3 \sum_{r=0}^3 \sum_{s=0}^3 \sum_{t=0}^3 \sum_{u=0}^3 \sum_{v=0}^3 \sum_{w=0}^3 \sum_{x=0}^3 \sum_{y=0}^3 \sum_{z=0}^3 \sum_{a=0}^3 \sum_{b=0}^3 \sum_{c=0}^3 \sum_{d=0}^3 \sum_{e=0}^3 \sum_{f=0}^3 \sum_{g=0}^3 \sum_{h=0}^3 \sum_{i=0}^3 \sum_{j=0}^3 \sum_{k=0}^3 \sum_{l=0}^3 \sum_{m=0}^3 \sum_{n=0}^3 \sum_{o=0}^3 \sum_{p=0}^3 \sum_{q=0}^3 \sum_{r=0}^3 \sum_{s=0}^3 \sum_{t=0}^3 \sum_{u=0}^3 \sum_{v=0}^3 \sum_{w=0}^3 \sum_{x=0}^3 \sum_{y=0}^3 \sum_{z=0}^3 \sum_{a=0}^3 \sum_{b=0}^3 \sum_{c=0}^3 \sum_{d=0}^3 \sum_{e=0}^3 \sum_{f=0}^3 \sum_{g=0}^3 \sum_{h=0}^3 \sum_{i=0}^3 \sum_{j=0}^3 \sum_{k=0}^3 \sum_{l=0}^3 \sum_{m=0}^3 \sum_{n=0}^3 \sum_{o=0}^3 \sum_{p=0}^3 \sum_{q=0}^3 \sum_{r=0}^3 \sum_{s=0}^3 \sum_{t=0}^3 \sum_{u=0}^3 \sum_{v=0}^3 \sum_{w=0}^3 \sum_{x=0}^3 \sum_{y=0}^3 \sum_{z=0}^3 \sum_{a=0}^3 \sum_{b=0}^3 \sum_{c=0}^3 \sum_{d=0}^3 \sum_{e=0}^3 \sum_{f=0}^3 \sum_{g=0}^3 \sum_{h=0}^3 \sum_{i=0}^3 \sum_{j=0}^3 \sum_{k=0}^3 \sum_{l=0}^3 \sum_{m=0}^3 \sum_{n=0}^3 \sum_{o=0}^3 \sum_{p=0}^3 \sum_{q=0}^3 \sum_{r=0}^3 \sum_{s=0}^3 \sum_{t=0}^3 \sum_{u=0}^3 \sum_{v=0}^3 \sum_{w=0}^3 \sum_{x=0}^3 \sum_{y=0}^3 \sum_{z=0}^3 \sum_{a=0}^3 \sum_{b=0}^3 \sum_{c=0}^3 \sum_{d=0}^3 \sum_{e=0}^3 \sum_{f=0}^3 \sum_{g=0}^3 \sum_{h=0}^3 \sum_{i=0}^3 \sum_{j=0}^3 \sum_{k=0}^3 \sum_{l=0}^3 \sum_{m=0}^3 \sum_{n=0}^3 \sum_{o=0}^3 \sum_{p=0}^3 \sum_{q=0}^3 \sum_{r=0}^3 \sum_{s=0}^3 \sum_{t=0}^3 \sum_{u=0}^3 \sum_{v=0}^3 \sum_{w=0}^3 \sum_{x=0}^3 \sum_{y=0}^3 \sum_{z=0}^3 \sum_{a=0}^3 \sum_{b=0}^3 \sum_{c=0}^3 \sum_{d=0}^3 \sum_{e=0}^3 \sum_{f=0}^3 \sum_{g=0}^3 \sum_{h=0}^3 \sum_{i=0}^3 \sum_{j=0}^3 \sum_{k=0}^3 \sum_{l=0}^3 \sum_{m=0}^3 \sum_{n=0}^3 \sum_{o=0}^3 \sum_{p=0}^3 \sum_{q=0}^3 \sum_{r=0}^3 \sum_{s=0}^3 \sum_{t=0}^3 \sum_{u=0}^3 \sum_{v=0}^3 \sum_{w=0}^3 \sum_{x=0}^3 \sum_{y=0}^3 \sum_{z=0}^3 \sum_{a=0}^3 \sum_{b=0}^3 \sum_{c=0}^3 \sum_{d=0}^3 \sum_{e=0}^3 \sum_{f=0}^3 \sum_{g=0}^3 \sum_{h=0}^3 \sum_{i=0}^3 \sum_{j=0}^3 \sum_{k=0}^3 \sum_{l=0}^3 \sum_{m=0}^3 \sum_{n=0}^3 \sum_{o=0}^3 \sum_{p=0}^3 \sum_{q=0}^3 \sum_{r=0}^3 \sum_{s=0}^3 \sum_{t=0}^3 \sum_{u=0}^3 \sum_{v=0}^3 \sum_{w=0}^3 \sum_{x=0}^3 \sum_{y=0}^3 \sum_{z=0}^3 \sum_{a=0}^3 \sum_{b=0}^3 \sum_{c=0}^3 \sum_{d=0}^3 \sum_{e=0}^3 \sum_{f=0}^3 \sum_{g=0}^3 \sum_{h=0}^3 \sum_{i=0}^3 \sum_{j=0}^3 \sum_{k=0}^3 \sum_{l=0}^3 \sum_{m=0}^3 \sum_{n=0}^3 \sum_{o=0}^3 \sum_{p=0}^3 \sum_{q=0}^3 \sum_{r=0}^3 \sum_{s=0}^3 \sum_{t=0}^3 \sum_{u=0}^3 \sum_{v=0}^3 \sum_{w=0}^3 \sum_{x=0}^3 \sum_{y=0}^3 \sum_{z=0}^3 \sum_{a=0}^3 \sum_{b=0}^3 \sum_{c=0}^3 \sum_{d=0}^3 \sum_{e=0}^3 \sum_{f=0}^3 \sum_{g=0}^3 \sum_{h=0}^3 \sum_{i=0}^3 \sum_{j=0}^3 \sum_{k=0}^3 \sum_{l=0}^3 \sum_{m=0}^3 \sum_{n=0}^3 \sum_{o=0}^3 \sum_{p=0}^3 \sum_{q=0}^3 \sum_{r=0}^3 \sum_{s=0}^3 \sum_{t=0}^3 \sum_{u=0}^3 \sum_{v=0}^3 \sum_{w=0}^3 \sum_{x=0}^3 \sum_{y=0}^3 \sum_{z=0}^3 \sum_{a=0}^3 \sum_{b=0}^3 \sum_{c=0}^3 \sum_{d=0}^3 \sum_{e=0}^3 \sum_{f=0}^3 \sum_{g=0}^3 \sum_{h=0}^3 \sum_{i=0}^3 \sum_{j=0}^3 \sum_{k=0}^3 \sum_{l=0}^3 \sum_{m=0}^3 \sum_{n=0}^3 \sum_{o=0}^3 \sum_{p=0}^3 \sum_{q=0}^3 \sum_{r=0}^3 \sum_{s=0}^3 \sum_{t=0}^3 \sum_{u=0}^3 \sum_{v=0}^3 \sum_{w=0}^3 \sum_{x=0}^3 \sum_{y=0}^3 \sum_{z=0}^3 \sum_{a=0}^3 \sum_{b=0}^3 \sum_{c=0}^3 \sum_{d=0}^3 \sum_{e=0}^3 \sum_{f=0}^3 \sum_{g=0}^3 \sum_{h=0}^3 \sum_{i=0}^3 \sum_{j=0}^3 \sum_{k=0}^3 \sum_{l=0}^3 \sum_{m=0}^3 \sum_{n=0}^3 \sum_{o=0}^3 \sum_{p=0}^3 \sum_{q=0}^3 \sum_{r=0}^3 \sum_{s=0}^3 \sum_{t=0}^3 \sum_{u=0}^3 \sum_{v=0}^3 \sum_{w=0}^3 \sum_{x=0}^3 \sum_{y=0}^3 \sum_{z=0}^3 \sum_{a=0}^3 \sum_{b=0}^3 \sum_{c=0}^3 \sum_{d=0}^3 \sum_{e=0}^3 \sum_{f=0}^3 \sum_{g=0}^3 \sum_{h=0}^3 \sum_{i=0}^3 \sum_{j=0}^3 \sum_{k=0}^3 \sum_{l=0}^3 \sum_{m=0}^3 \sum_{n=0}^3 \sum_{o=0}^3 \sum_{p=0}^3 \sum_{q=0}^3 \sum_{r=0}^3 \sum_{s=0}^3 \sum_{t=0}^3 \sum_{u=0}^3 \sum_{v=0}^3 \sum_{w=0}^3 \sum_{x=0}^3 \sum_{y=0}^3 \sum_{z=0}^3 \sum_{a=0}^3 \sum_{b=0}^3 \sum_{c=0}^3 \sum_{d=0}^3 \sum_{e=0}^3 \sum_{f=0}^3 \sum_{g=0}^3 \sum_{h=0}^3 \sum_{i=0}^3 \sum_{j=0}^3 \sum_{k=0}^3 \sum_{l=0}^3 \sum_{m=0}^3 \sum_{n=0}^3 \sum_{o=0}^3 \sum_{p=0}^3 \sum_{q=0}^3 \sum_{r=0}^3 \sum_{s=0}^3 \sum_{t=0}^3 \sum_{u=0}^3 \sum_{v=0}^3 \sum_{w=0}^3 \sum_{x=0}^3 \sum_{y=0}^3 \sum_{z=0}^3 \sum_{a=0}^3 \sum_{b=0}^3 \sum_{c=0}^3 \sum_{d=0}^3 \sum_{e=0}^3 \sum_{f=0}^3 \sum_{g=0}^3 \sum_{h=0}^3 \sum_{i=0}^3 \sum_{j=0}^3 \sum_{k=0}^3 \sum_{l=0}^3 \sum_{m=0}^3 \sum_{n=0}^3 \sum_{o=0}^3 \sum_{p=0}^3 \sum_{q=0}^3 \sum_{r=0}^3 \sum_{s=0}^3 \sum_{t=0}^3 \sum_{u=0}^3 \sum_{v=0}^3 \sum_{w=0}^3 \sum_{x=0}^3 \sum_{y=0}^3 \sum_{z=0}^3 \sum_{a=0}^3 \sum_{b=0}^3 \sum_{c=0}^3 \sum_{d=0}^3 \sum_{e=0}^3 \sum_{f=0}^3 \sum_{g=0}^3 \sum_{h=0}^3 \sum_{i=0}^3 \sum_{j=0}^3 \sum_{k=0}^3 \sum_{l=0}^3 \sum_{m=0}^3 \sum_{n=0}^3 \sum_{o=0}^3 \sum_{p=0}^3 \sum_{q=0}^3 \sum_{r=0}^3 \sum_{s=0}^3 \sum_{t=0}^3 \sum_{u=0}^3 \sum_{v=0}^3 \sum_{w=0}^3 \sum_{x=0}^3 \sum_{y=0}^3 \sum_{z=0}^3 \sum_{a=0}^3 \sum_{b=0}^3 \sum_{c=0}^3 \sum_{d=0}^3 \sum_{e=0}^3 \sum_{f=0}^3 \sum_{g=0}^3 \sum_{h=0}^3 \sum_{i=0}^3 \sum_{j=0}^3 \sum_{k=0}^3 \sum_{l=0}^3 \sum_{m=0}^3 \sum_{n=0}^3 \sum_{o=0}^3 \sum_{p=0}^3 \sum_{q=0}^3 \sum_{r=0}^3 \sum_{s=0}^3 \sum_{t=0}^3 \sum_{u=0}^3 \sum_{v=0}^3 \sum_{w=0}^3 \sum_{x=0}^3 \sum_{y=0}^3 \sum_{z=0}^3 \sum_{a=0}^3 \sum_{b=0}^3 \sum_{c=0}^3 \sum_{d=0}^3 \sum_{e=0}^3 \sum_{f=0}^3 \sum_{g=0}^3 \sum_{h=0}^3 \sum_{i=0}^3 \sum_{j=0}^3 \sum_{k=0}^3 \sum_{l=0}^3 \sum_{m=0}^3 \sum_{n=0}^3 \sum_{o=0}^3 \sum_{p=0}^3 \sum_{q=0}^3 \sum_{r=0}^3 \sum_{s=0}^3 \sum_{t=0}^3 \sum_{u=0}^3 \sum_{v=0}^3 \sum_{w=0}^3 \sum_{x=0}^3 \sum_{y=0}^3 \sum_{z=0}^3 \sum_{a=0}^3 \sum_{b=0}^3 \sum_{c=0}^3 \sum_{d=0}^3 \sum_{e=0}^3 \sum_{f=0}^3 \sum_{g=0}^3 \sum_{h=0}^3 \sum_{i=0}^3 \sum_{j=0}^3 \sum_{k=0}^3 \sum_{l=0}^3 \sum_{m=0}^3 \sum_{n=0}^3 \sum_{o=0}^3 \sum_{p=0}^3 \sum_{q=0}^3 \sum_{r=0}^3 \sum_{s=0}^3 \sum_{t=0}^3 \sum_{u=0}^3 \sum_{v=0}^3 \sum_{w=0}^3 \sum_{x=0}^3 \sum_{y=0}^3 \sum_{z=0}^3 \sum_{a=0}^3 \sum_{b=0}^3 \sum_{c=0}^3 \sum_{d=0}^3 \sum_{e=0}^3 \sum_{f=0}^3 \sum_{g=0}^3 \sum_{h=0}^3 \sum_{i=0}^3 \sum_{j=0}^3 \sum_{k=0}^3 \sum_{l=0}^3 \sum_{m=0}^3 \sum_{n=0}^3 \sum_{o=0}^3 \sum_{p=0}^3 \sum_{q=0}^3 \sum_{r=0}^3 \sum_{s=0}^3 \sum_{t=0}^3 \sum_{u=0}^3 \sum_{v=0}^3 \sum_{w=0}^3 \sum_{x=0}^3 \sum_{y=0}^3 \sum_{z=0}^3 \sum_{a=0}^3 \sum_{b=0}^3 \sum_{c=0}^3 \sum_{d=0}^3 \sum_{e=0}^3 \sum_{f=0}^3 \sum_{g=0}^3 \sum_{h=0}^3 \sum_{i=0}^3 \sum_{j=0}^3 \sum_{k=0}^3 \sum_{l=0}^3 \sum_{m=0}^3 \sum_{n=0}^3 \sum_{o=0}^3 \sum_{p=0}^3 \sum_{q=0}^3 \sum_{r=0}^3 \sum_{s=0}^3 \sum_{t=0}^3 \sum_{u=0}^3 \sum_{v=0}^3 \sum_{w=0}^3 \sum_{x=0}^3 \sum_{y=0}^3 \sum_{z=0}^3 \sum_{a=0}^3 \sum_{b=0}^3 \sum_{c=0}^3 \sum_{d=0}^3 \sum_{e=0}^3 \sum_{f=0}^3 \sum_{g=0}^3 \sum_{h=0}^3 \sum_{i=0}^3 \sum_{j=0}^3 \sum_{k=0}^3 \sum_{l=0}^3 \sum_{m=0}^3 \sum_{n=0}^3 \sum_{o=0}^3 \sum_{p=0}^3 \sum_{q=0}^3 \sum_{r=0}^3 \sum_{s=0}^3 \sum_{t=0}^3 \sum_{u=0}^3 \sum_{v=0}^3 \sum_{w=0}^3 \sum_{x=0}^3 \sum_{y=0}^3 \sum_{z=0}^3 \sum_{a=0}^3 \sum_{b=0}^3 \sum_{c=0}^3 \sum_{d=0}^3 \sum_{e=0}^3 \sum_{f=0}^3 \sum_{g=0}^3 \sum_{h=0}^3 \sum_{i=0}^3 \sum_{j=0}^3 \sum_{k=0}^3 \sum_{l=0}^3 \sum_{m=0}^3 \sum_{n=0}^3 \sum_{o=0}^3 \sum_{p=0}^3 \sum_{q=0}^3 \sum_{r=0}^3 \sum_{s=0}^3 \sum_{t=0}^3 \sum_{u=0}^3 \sum_{v=0}^3 \sum_{w=0}^3 \sum_{x=0}^3 \sum_{y=0}^3 \sum_{z=0}^3 \sum_{a=0}^3 \sum_{b=0}^3 \sum_{c=0}^3 \sum_{d=0}^3 \sum_{e=0}^3 \sum_{f=0}^3 \sum_{g=0}^3 \sum_{h=0}^3 \sum_{i=0}^3 \sum_{j=0}^3 \sum_{k=0}^3 \sum_{l=0}^3 \sum_{m=0}^3 \sum_{n=0}^3 \sum_{o=0}^3 \sum_{p=0}^3 \sum_{q=0}^3 \sum_{r=0}^3 \sum_{s=0}^3 \sum_{t=0}^3 \sum_{u=0}^3 \sum_{v=0}^3 \sum_{w=0}^3 \sum_{x=0}^3 \sum_{y=0}^3 \sum_{z=0}^3 \sum_{a=0}^3 \sum_{b=0}^3 \sum_{c=0}^3 \sum_{d=0}^3 \sum_{e=0}^3 \sum_{f=0}^3 \sum_{g=0}^3 \sum_{h=0}^3 \sum_{i=0}^3 \sum_{j=0}^3 \sum_{k=0}^3 \sum_{l=0}^3 \sum_{m=0}^3 \sum_{n=0}^3 \sum_{o=0}^3 \sum_{p=0}^3 \sum_{q=0}^3 \sum_{r=0}^3 \sum_{s=0}^3 \sum_{t=0}^3 \sum_{u=0}^3 \sum_{v=0}^3 \sum_{w=0}^3 \sum_{x=0}^3 \sum_{y=0}^3 \sum_{z=0}^3 \sum_{a=0}^3 \sum_{b=0}^3 \sum_{c=0}^3 \sum_{d=0}^3 \sum_{e=0}^3 \sum_{f=0}^3 \sum_{g=0}^3 \sum_{h=0}^3 \sum_{i=0}^3 \sum_{j=0}^3 \sum_{k=0}^3 \sum_{l=0}^3 \sum_{m=0}^3 \sum_{n=0}^3 \sum_{o=0}^3 \sum_{p=0}^3 \sum_{q=0}^3 \sum_{r=0}^3 \sum_{s=0}^3 \sum_{t=0}^3 \sum_{u=0}^3 \sum_{v=0}^3 \sum_{w=0}^3 \sum_{x=0}^3 \sum_{y=0}^3 \sum_{z=0}^3 \sum_{a=0}^3 \sum_{b=0}^3 \sum_{c=0}^3 \sum_{d=0}^3 \sum_{e=0}^3 \sum_{f=0}^3 \sum_{g=0}^3 \sum_{h=0}^3 \sum_{i=0}^3 \sum_{j=0}^3 \sum_{k=0}^3 \sum_{l=0}^3 \sum_{m=0}^3 \sum_{n=0}^3 \sum_{o=0}^3 \sum_{p=0}^3 \sum_{q=0}^3 \sum_{r=0}^3 \sum_{s=0}^3 \sum_{t=0}^3 \sum_{u=0}^3 \sum_{v=0}^3 \sum_{w=0}^3 \sum_{x=0}^3 \sum_{y=0}^3 \sum_{z=0}^3 \sum_{a=0}^3 \sum_{b=0}^3 \sum_{c=0}^3 \sum_{d=0}^3 \sum_{e=0}^3 \sum_{f=0}^3 \sum_{g=0}^3 \sum_{h=0}^3 \sum_{i=0}^3 \sum_{j=0}^3 \sum_{k=0}^3 \sum_{l=0}^3 \sum_{m=0}^3 \sum_{n=0}^3 \sum_{o=0}^3 \sum_{p=0}^3 \sum_{q=0}^3 \sum_{r=0}^3 \sum_{s=0}^3 \sum_{t=0}^3 \sum_{u=0}^3 \sum_{v=0}^3 \sum_{w=0}^3 \sum_{x=0}^3 \sum_{y=0}^3 \sum_{z=0}^3 \sum_{a=0}^3 \sum_{b=0}^3 \sum_{c=0}^3 \sum_{d=0}^3 \sum_{e=0}^3 \sum_{f=0}^3 \sum_{g=0}^3 \sum_{h=0}^3 \sum_{i=0}^3 \sum_{j=0}^3 \sum_{k=0}^3 \sum_{l=0}^3 \sum_{m=0}^3 \sum_{n=0}^3 \sum_{o=0}^3 \sum_{p=0}^3 \sum_{q=0}^3 \sum_{r=0}^3 \sum_{s=0}^3 \sum_{t=0}^3 \sum_{u=0}^3 \sum_{v=0}^3 \sum_{w=0}^3 \sum_{x=0}^3 \sum_{y=0}^3 \sum_{z=0}^3 \sum_{a=0}^3 \sum_{b=0}^3 \sum_{c=0}^3 \sum_{d=0}^3 \sum_{e=0}^3 \sum_{f=0}^3 \sum_{g=0}^3 \sum_{h=0}^3 \sum_{i=0}^3 \sum_{j=0}^3 \sum_{k=0}^3 \sum_{l=0}^3 \sum_{m=0}^3 \sum_{n=0}^3 \sum_{o=0}^3 \sum_{p=0}^3 \sum_{q=0}^3 \sum_{r=0}^3 \sum_{s=0}^3 \sum_{t=0}^3 \sum_{u=0}^3 \sum_{v=0}^3 \sum_{w=0}^3 \sum_{x=0}^3 \sum_{y=0}^3 \sum_{z=0}^3 \sum_{a=0}^3 \sum_{b=0}^3 \sum_{c=0}^3 \sum_{d=0}^3 \sum_{e=0}^3 \sum_{f=0}^3 \sum_{g=0}^3 \sum_{h=0}^3 \sum_{i=0}^3 \sum_{j=0}^3 \sum_{k=0}^3 \sum_{l=0}^3 \sum_{m=0}^3 \sum_{n=0}^3 \sum_{o=0}^3 \sum_{p=0}^3 \sum_{q=0}^3 \sum_{r=0}^3 \sum_{s=0}^3 \sum_{t=0}^3 \sum_{u=0}^3 \sum_{v=0}^3 \sum_{w=0}^3 \sum_{x=0}^3 \sum$$

resentation  $G = A L A^{-1}$ , acting in  $\mathbb{C}^2$  reads

$$G = \frac{1}{2} \begin{bmatrix} 1 + \cos \theta & 1 - \cos \theta & \sin \theta & \sin \theta \\ 1 - \cos \theta & 1 + \cos \theta & \sin \theta & \sin \theta \\ \sin \theta & \sin \theta & 1 + \cos \theta & 1 - \cos \theta \\ \sin \theta & \sin \theta & 1 - \cos \theta & 1 + \cos \theta \end{bmatrix} : \begin{bmatrix} 0 & 1 \\ 1 & 0 \end{bmatrix} \begin{bmatrix} B & C \\ C & A \end{bmatrix} \begin{bmatrix} 0 & 1 \\ 1 & 0 \end{bmatrix}$$

The results presented in Fig. 2 are averages over 36 rotation angles evenly spaced across the entire interval  $[0; 2\pi]$ . The best performance was observed for  $\theta = 0$  (identity) and  $\theta = \pi$ , while the worst cases were encountered around  $\theta = \pi/2$  (but not exactly at these angles). For each setting  $(\theta, \gamma)$ , the inhibition level  $\eta$  was adjusted to minimize the variance of fidelity across the test states and rotation angles (cf. Fig. 2-insets). Note that while this optimization was mainly coincident with maximization of the fidelity itself, the trend in coherence was typically opposite. Had we chosen to optimize for purity of states ( $R = 1$ ), the figures would look different.

The prominent feature of Fig. 2a, is the overcoherence of output states in the limit  $\gamma \rightarrow 0$ . This means these distributions are too sharp to represent quantum states, and any subsequent application of another gate would certainly lead to a loss of accuracy. Interestingly, the average fidelity remains at relatively high level. This suggests a possibility of correcting the distributions by rescaling about the average. On the other hand, the fidelity SD is significant for small saturations, and becomes comparable with statistical uncertainties only above  $\gamma \approx 1$ .

The conclusion of Fig. 2b is rather clear: the circuit considered here is designed to work in deterministic regime  $\gamma \neq 0$ . This makes an interesting contrast between stochastic nature of quantum states and the determinism of gates acting on them. As we are going to show, this dichotomy is not limited to the 1-qubit gate, but persists also in the case of entangling operation CNOT.

Finally, we have sought an estimate of the time needed to complete the quantum rotations with this gate. Apart from the spatial resources, measured in terms of cells and connections being used, time is an important factor contributing to the overall cost of the realization. To assess this property, we have run the circuit while varying the *signal length*  $\tau_{\text{sig}}$ : After an initial transient of  $\tau_{\text{gate}} = 4 + \tau_{\text{avr}}$ , the network was ran for  $\tau_{\text{sig}} > 1$  successive steps, after which the cells were re-set to their initial state ( $u^i = 0, X^i = 0$ ), ensuring that all memory traces stored in latent potentials were erased. This procedure was repeated until satisfactory statistics ( $N_{\text{sig}} = 10^4$ ) was gathered.

The results provided in Fig. 2c evidently show that the real temporal cost is not only the delay  $\tau_{\text{gate}}$ , but a significant number of further steps are needed to 'tune' this gate to a signal. After approximately  $\tau_{\text{sig}} \approx 30$  events the output quality no longer improves, and consequently one can identify  $\tau_{\text{sig}}$  with the statistics needed for maximal efficiency. Since the latter is a function of saturation  $\gamma$  and noise  $\sigma$ , one expects  $\tau_{\text{sig}}$  to raise mono-

tonically with  $\gamma$  and decrease as  $\sigma$  increases. In particular, the ideal case  $\gamma = 1, \sigma = 0$  would also require infinite statistics to achieve the best performance. One therefore finds yet another reason for the low saturation values: The finiteness of signals encoded in spike trains, limits the attainable efficiency of transformations, and high saturation values cannot provide improvement beyond these limitations.

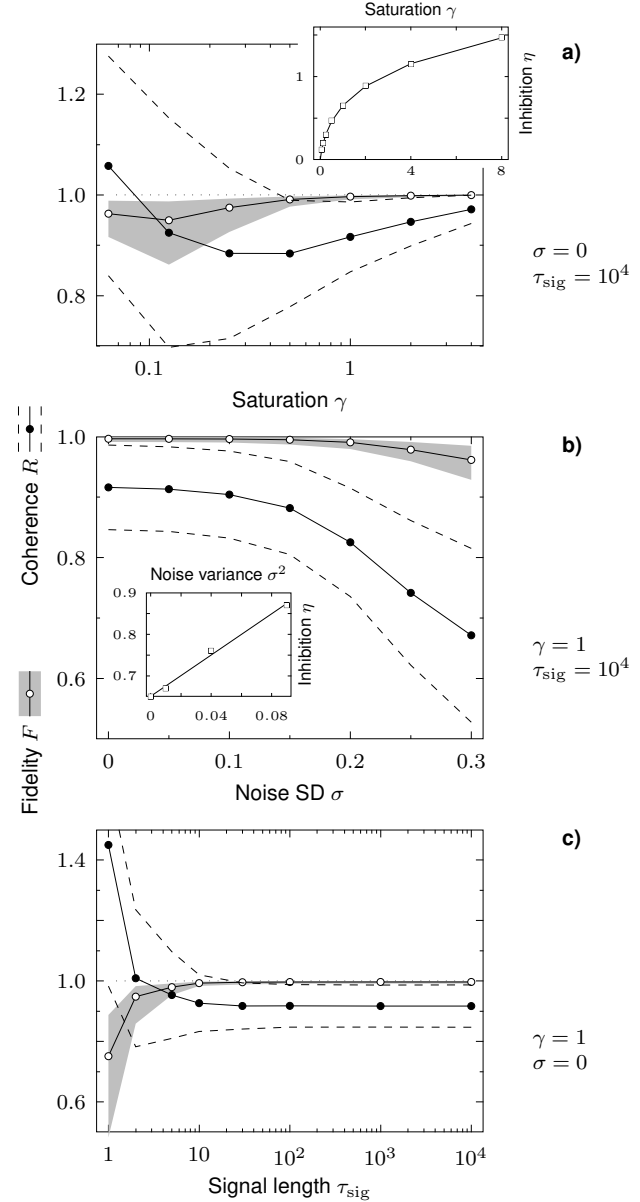


**Figure 2** Performance of the 1-qubit phase gate in function of **a**): saturation level of the latent potential, **b**): noise SD of the activation function  $P$ , **c**): length of the input signal (note the scale difference between graphs). Synaptic averaging was fixed at  $\tau_{\text{avr}} = 2$ . Each point is a mean over 36 rotation angles within the whole interval  $[0; 2\pi]$ , and 14 pure states on which the phase gate was tested. With statistics of  $10^4$  steps per setting, the associated uncertainties are negligible – shaded regions ( $F$ ) and broken lines ( $R$ ) represent the standard deviations across the states and rotation angles. **Inset**: The inhibition levels used during simulations, optimized for minimization of the fidelity variance.

## 4.2 The CNOT gate

Unlike the single-qubit gates which can, by means of a special choice of the POVM, be transformed to a permutation, the CNOT operation does not admit such representation<sup>5</sup>. With  $A$  given by (6), its operator  $G_{\text{CNOT}} = A L_{\text{CNOT}} A^{-1}$  has the following structure

$$G_{\text{CNOT}} = \begin{pmatrix} 0 & H_1 & J_1 & H_1^T + J_2 & H_2 & H_2^T & 1 \\ \overline{B} & H_1^T + J_2 & H_1 & J_1 & H_2^T & H_2 & \overline{C} \\ \overline{B} & \overline{B} & H_2 & H_2^T & H_1 & J_2 & H_1^T + J_1 A \\ \overline{B} & \overline{B} & H_2^T & H_2 & H_1^T + J_1 & H_1 & J_2 \end{pmatrix};$$

where

$$\begin{aligned} H_1 &= \frac{1}{4} \begin{pmatrix} 0 & 1 & \frac{1}{3} & 1 & \frac{1}{3} & 1 \\ \overline{B} & 1 & \frac{1}{3} & 1 & \frac{1}{3} & \overline{C} \\ \overline{B} & \frac{1}{3} & 1 & \frac{1}{3} & 1 & \frac{1}{3} A \\ \overline{B} & \frac{1}{3} & 1 & \frac{1}{3} & 1 & \frac{1}{3} \\ \overline{B} & \frac{1}{3} & 1 & \frac{1}{3} & 1 & 1 \end{pmatrix}; \\ H_2 &= \frac{1}{4} \begin{pmatrix} 0 & \frac{1}{3} & 1 & \frac{1}{3} & 1 & 1 \\ \overline{B} & 1 & \frac{1}{3} & 1 & \frac{1}{3} & \overline{C} \\ \overline{B} & \frac{1}{3} & 1 & \frac{1}{3} & 1 & \frac{1}{3} A \\ \overline{B} & \frac{1}{3} & 1 & \frac{1}{3} & 1 & \frac{1}{3} \\ \overline{B} & \frac{1}{3} & 1 & \frac{1}{3} & 1 & 1 \end{pmatrix}; \\ J_1 &= \frac{1}{3} \begin{pmatrix} 0 & B & 0 & 0 & 0 & 1 \\ \overline{B} & 0 & 0 & 0 & 1 & \overline{C} \\ \overline{B} & 0 & 0 & 1 & 0 & A \\ \overline{B} & 0 & 1 & 0 & 0 & 1 \\ \overline{B} & 0 & 0 & 1 & 0 & 0 \\ \overline{B} & 0 & 0 & 0 & 1 & 0 \end{pmatrix}; \\ J_2 &= \frac{1}{3} \begin{pmatrix} 0 & B & 0 & 1 & 0 & 0 \\ \overline{B} & 0 & 1 & 0 & 0 & C \\ \overline{B} & 1 & 0 & 0 & 0 & A \\ \overline{B} & 0 & 0 & 0 & 1 & 0 \\ \overline{B} & 0 & 0 & 0 & 0 & 1 \end{pmatrix}; \end{aligned}$$

As already mentioned, the POVM (6) has been chosen to optimize the CNOT gate. Indeed, the linear projection

$$W = \begin{pmatrix} 0 & 0 & 0 & 0 & 0 & \dots & 1 & 1 \\ \overline{B} & 0 & 0 & 0 & 1 & \dots & 1 & \overline{C} \\ \overline{B} & 0 & 0 & 1 & 1 & \dots & 1 & \overline{A} \\ \overline{B} & 0 & 1 & 0 & 1 & \dots & 0 & 1 \end{pmatrix};$$

when combined with  $G_{\text{CNOT}}$ , shows the two pbits  $X^A$  and  $X^D$  are invariant under  $G_{\text{CNOT}}$ . These can be directly copied to the output  $X^A$ ,  $X^D$ , as shown in Fig. 3. For that same reason, while implementing the embedding part<sup>1</sup>, we pair  $fX^A; X^D g; fX^B; X^C g$ , rather than using the natural order  $fX^A; X^B g; fX^C; X^D g$ . The section<sup>1</sup> is a two-stage procedure: First, with the same construction as in 1-qubit case we separately embed the two marginals  $fX^A; X^D g$  and  $fX^B; X^C g$ .

$$\Pi^1 : V^4 ! \quad 2 \quad 2 :$$

Next, we combine these into a single map

$$\Pi^1 : \quad 2 \quad 2 ! \quad 4 :$$

<sup>5</sup>Would it be possible, then either the gate could have no entangling capability, or the marginal probabilities of the two qubits be not conserved.

Since this is done with a linear mapping, there is again a rectifying feedback  $W_{\text{rec};\Pi}$  obtainable from Eq. (7) applied to  $\Pi$  on  $V^4$ . In contrast to  $\Pi^1$ , the second-stage embedding  $\Pi^1$  turns out to be unstable against noise, and the normalization feedback is now a necessity. Because of

$$8i 2^4 \sum_j W_{\text{rec};\Pi}^i j = \frac{9}{16} S(-1);$$

the normalization weights are set to

$$W_{\text{nor};\Pi} = 9S(-1)(D_4 - 1);$$

where  $D_4 j$  is the diffusion operator, and '1' refers to the unit vertex  $\nabla_1$ .

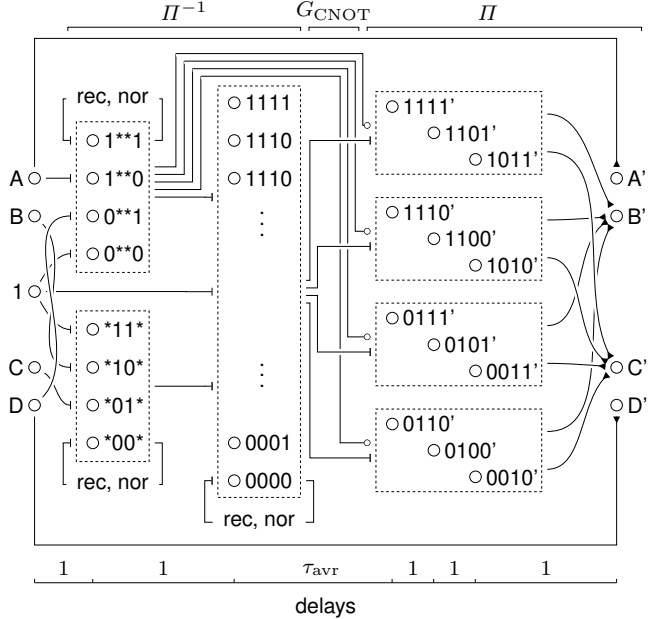


**Figure 3** Schematic of the CNOT gate. The circuit has 38 nodes, and 1309 edges if the synaptic averaging is set to  $\text{avr} = 4$ . The transient time is  $\text{gate} = 5 + \text{avr}$ .

Thanks to the invariance of two pbits  $X^A = X^A$ ,  $X^D = X^D$ , the hierarchical projection have been significantly simplified (in comparison to what is needed for general 2-qubit gate). The four partial projections from  $G_{\text{CNOT}}$ , shown on the right hand side of Fig. 3, are modulated directly by the marginal  $\Pi^1(X^A; X^D)$ . The mechanism of this modulation is the same as explained before (inhibition followed by attenuated excitation) and the same parameter is set common on those connections.

Finally, the gate edges were multiplied, in order to use the synaptic averaging mechanism. We found no dramatic improvement while varying the averaging length  $\text{avr}$ , at  $\text{avr} = 1$ , nevertheless the performance was significantly better for small values of the saturation parameter. At  $\text{avr} = 1$  the optimal length was  $\text{avr} = 4$ .

**Results.** The performance was assessed upon a testing set of 28 pure states, which included both separable and entangled ones:

$$\begin{aligned}
 & \text{J00i; J01i; J10i; J11i;} \\
 & \frac{1}{2} \text{ J00i} + e^{ik} \frac{1}{2} \text{ J01i} ; \quad \frac{1}{2} \text{ J00i} + e^{ik} \frac{1}{2} \text{ J10i} ; \\
 & \frac{1}{2} \text{ J00i} + e^{ik} \frac{1}{2} \text{ J11i} ; \quad \frac{1}{2} \text{ J01i} + e^{ik} \frac{1}{2} \text{ J10i} ; \\
 & \frac{1}{2} \text{ J01i} + e^{ik} \frac{1}{2} \text{ J11i} ; \quad \frac{1}{2} \text{ J10i} + e^{ik} \frac{1}{2} \text{ J11i} ;
 \end{aligned}$$

$k \in \mathbb{Z}_4$

Interestingly, although some of these states are 'preferred' in terms of achieved fidelity  $F$ , there was no correlation between this measure and the entanglement property.

Like before, for each setting ( $\gamma$ ,  $\sigma$ ), the inhibition level was adjusted to minimize the variance of fidelity. The results are presented in Fig. 4.

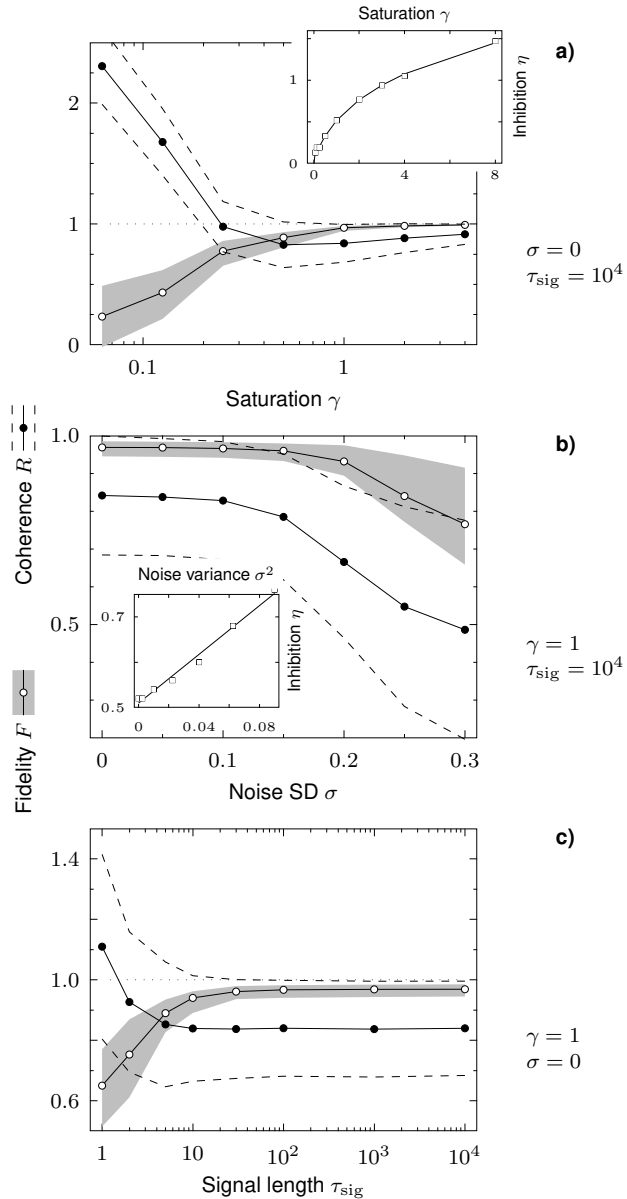


**Figure 4** Performance of the CNOT gate for synaptic averaging fixed at  $\text{avr} = 4$ . Note the differences in ranges, while comparing with Fig. 2. The statistics for each setting is  $10^4$  steps, and each point is an average over 28 test states.

Qualitatively, these are largely similar to what had been obtained for 1-qubit gates, the major difference between Figs. 2 and 4 is in the range of achieved fidelities and output coherence. Standard deviations of coherence  $R$  increased evenly by approximately a factor of 2, while the fidelity SD multiplied by about 4–5. The most dramatic changes are observed in Fig. 4a: Whereas at low saturation values ( $\gamma < 1$ ) the 1-qubit gate worked relatively well, in the case of CNOT a huge overcoherence takes place along with significant fidelity loss.

For a reasonable performance at  $\gamma = 0$  and  $\sigma_{\text{sig}} = 30$  one needs  $\eta \approx 1$ . In this regime one finds  $F \approx 0.97$  ( $0.03;+0.02$ ), corresponding to the unitary error  $\approx 0.14$  ( $5;+4$ ); with noise at  $\sigma = 0.3$  and  $\eta = 1$  the fidelity drops down to  $F = 0.77$  ( $0.11;+0.15$ ), or  $\eta = 42$  ( $22;+12$ ), what is hardly acceptable for a large-scale quantum computation. While comparing these values with the best to-date experimental achievements ( $F = 0.7\text{--}0.8$  with trapped ions [13],  $F = 0.6\text{--}0.8$  with Josephson junctions [14],  $F = 0.85$  in optical setup [15]) one has to take into account the many simplifications of our toy-model. More realistic realizations may not necessarily prove as good as this one, nevertheless the principle has been demonstrated.

## 5 Discussion

We have studied the potential of an artificial neural network to operate on correlated spike trains assuming the latter to encode quantum states. The model neurons are reduced here down to the essential ingredients of computational capability. Out of these simplifications several may however make the hypothesized processing scheme questionable in real networks: First, while the presence of a latent (residual) potential, which was shown to be crucial for unitary transformations, is in itself an acceptable feature, one can argue against our tacit assumption concerning its variability. Namely, we have imposed no constraints on the rate at which this potential can change. If one makes an identification with the 'base' membrane potential (in between consecutive spikes), then the physiological recordings suggests it fluctuates on a much longer time-scale than the minimal interspike distance. Second, we have completely neglected the synaptic noise, by assuming the signals to be relayed undisturbed between cells. The justification is that here the few edges of each node represent averages over  $10^3\text{--}10^4$  real synaptic connections and the impact of a faulty transmission through a single synapse is reduced. But inclusion of this likely source of errors may still be a significant factor reducing the overall performance. Third, the binary-output model ignores the irregularities in action potentials. By taking this element into account one has to regard it either as an active information carrier (preferably), or as an uncertainty factor contributing to the noise and effectively decreasing the performance.

As it has already been mentioned, the proposed circuits are designed to work in the deterministic regime. The underlying idea is that of a neuron acting as a ‘counter’ which discretizes the accumulated input signal. Existence of a sharp firing threshold needed for this construction corroborates with the theoretical analysis of optimality in terms of information encoding [20]. On the other hand, the noise itself which blurs this threshold has been shown to be a viable resource acting through the mechanisms of stochastic resonance [21]. Whereas we have converted the dense code into *spatial* sparse code before quantum transformations could be applied, the models which use stochastic resonance operate on *temporal* sparse coding<sup>6</sup>. In favor of the latter speaks a good agreement between the theory and recordings from sensory neurons [22], presence of many brain rhythms which may serve as reference waves or ‘clocks’ necessary in this form of a code, and experimental studies [23, 24], which show relative phase to be an independent variable in information transmission. But one should be cautious in adopting temporal encoding in the circuits, at least for one reason: The mechanisms of short-term synaptic plasticity [18, 19], which are predisposed to detect causality, and hence – correlations in spike trains [27], can severely impart the delicate alignment of synaptic couplings needed for quantum transformations. In this context, the use of spatial coding, which is also found in the cortex [25, 26] appears to be an advantage, for such spike trains have by definition no temporal correlations, and hence the circuits operating in this fashion are expected to be more stable.

In conclusion, we have demonstrated the principle of employing quantum coding in artificial neural networks, by providing examples of circuits which realize quantum gates. There is a room for improvement and further investigation with more realism put into the model, alternative circuits, and algorithm implementations. Exploring the possible ways in which neural networks can handle quantum codes, can certainly benefit both the quantum mechanics and neuroscience. On the one hand, applications of QM to neural systems broaden the range of possibilities to be considered when seeking to understand the language of spikes, on the other – macroscopic realizations can provide clues about the microscopic phenomena upon which QM originated.

## References

- [1] F. Rieke, D. Warland, R.R. de Ruyter van Steveninck, W. Bialek, “*Spikes: Exploring the Neural Code*”, The MIT Press, Cambridge, Massachusetts 1997.
- [2] P.S. Churchland, T.J. Sejnowski, “*The Computational Brain*”, The MIT Press, Cambridge, Massachusetts 1992.
- [3] D. Aerts, “*A possible explanation for the probabilities of quantum mechanics*”, *J. Math. Phys.* **27** (1986), 202–210.
- [4] D. Aerts, M. Czachor, “*Bag-of-words problem and semantic analysis in Fock space*”, *quant-ph/0309022*
- [5] D.C. Brody, “*Shapes of quantum states*”, *J. Phys. A: Math. Gen.* **37** (2004), 251–257.
- [6] L.E. Ballentine, “*The statistical interpretation of quantum mechanics*”, *Rev. Mod. Phys.* **42**:2 (1970), 358–381.
- [7] A. Peres, “*Quantum Theory: Concepts and Methods*”, Kluwer Academic Publishers, Dordrecht 1995.
- [8] A. Peres, D.R. Terno, “*Convex probability domain of generalized quantum measurements*”, *J. Phys. A* **31** (1998), L671–L675.
- [9] C.M. Caves, Ch.A. Fuchs, R. Schack, “*Quantum probabilities as Bayesian probabilities*”, *Phys. Rev. A* **65** (2002), 022305.
- [10] V. Bužek, M. Hillery, R.F. Werner, “*Optimal manipulations with qubits: Universal-NOT gate*”, *Phys. Rev. A* **60** (1999), R2626–9.
- [11] F. De Martini, V. Bužek, F. Sciarrino, C. Sias, “*Experimental realization of the quantum universal NOT gate*”, *Nature* **419** (2002), 815–818.
- [12] A. Barenco, C.H. Bennett, R. Cleve, D.P. DiVincenzo, N. Margolus, P. Shor, T. Sleator, J.A. Smolin, H. Weinfurter, “*Elementary gates for quantum computation*”, *Phys. Rev. A* **52** (1995), 3457–3467.
- [13] F. Schmidt-Kaler, *et al.* “*Realization of the Cirac-Zoller controlled-NOT quantum gate*”, *Nature* **422** (2003), 408–411.
- [14] T. Yamamoto, Yu.A. Pashkin, O. Astafiev, Y. Nakamura, J.S. Tsai, “*Demonstration of conditional gate operation using superconducting charge qubits*”, *Nature* **425** (2003), 941–946.
- [15] J.L. O’Brien, G.J. Pryde, A.G. White, T.C. Ralph, “*Demonstration of an all-optical quantum controlled-NOT gate*”, *Nature* **426** (2003), 264–267.
- [16] M. Carandini, D. Heeger, J.A. Movshon, “*Linearity and normalization in simple cells of the macaque primary visual cortex*”, *J. Neurosci.* **17** (1997), 8621–8644.
- [17] G.G. Turrigiano, K.R. Leslie, N.S. Desai, L.C. Rutheford, S.B. Nelson, “*Activity-dependent scaling of quantal amplitude in neocortical neurons*”, *Nature* **391** (1998), 892–896.
- [18] H. Makram, J. Lubke, M. Frotscher, B. Sakmann, “*Regulation of synaptic efficacy by coincidence of postsynaptic SPs and EPSPs*”, *Science* **275** (1997), 213–215.
- [19] R.C. Froemke, Y. Dan, “*Spike-timing-dependent synaptic modification induced by natural spike trains*”, *Nature* **416** (2002), 433–438.
- [20] M. Bethge, D. Rotermund, K. Pawelzik, “*Optimal neural rate coding leads to bimodal firing rate distributions*”, *Network: Comput. Neural Syst.* **14** (2003), 303–319.
- [21] L. Gammaconi, P. Hänggi, P. Jung, F. Marchesoni, “*Stochastic resonance*”, *Rev. Mod. Phys.* **70** (1998), 223–287.
- [22] “*Stochastic resonance on a circle*”, K. Wiesenfeld, D. Pierson, E. Pantazelou, C. Dames, F. Moss, *Phys. Rev. Lett.* **72** (1994), 2125–2129.
- [23] M.W. Oram, D. Xiao, B. Dritschel, K.R. Payne, “*The temporal resolution of neural codes: does response latency have a unique role?*”, *Phil. Trans. R. Soc. Lond. B* **357** (2002), 987–1001.
- [24] J. Huxter, N. Burgess, J. O’Keefe, “*Independent rate and temporal coding in hippocampal pyramidal cells*”, *Nature* **425** (2003), 828–832.
- [25] A. Arieli, A. Sterkin, A. Grinvald, A. Aertsen, “*Dynamics of ongoing activity: Explanation of the large variability in evoked cortical responses*”, *Science* **273** (1996), 1868–1871.
- [26] T. Kenet, D. Bibitchkov, M. Tsodyks, A. Grinvald, A. Arieli, “*Spontaneously emerging cortical representations of visual attributes*”, *Nature* **425** (2003), 954–956.
- [27] A.L. Fairhall, G.D. Lewen, W. Bialek, R.R. de Ruyter van Steveninck, “*Efficiency and ambiguity in an adaptive neural code*”, *Nature* **412** (2001), 787–792

<sup>6</sup>By ‘temporal sparse code’ we understand probability waves, which should not to be confused with temporal response of a circuit to static spatial stimulus.